T. Oshima, M. Imano, A full finite-volume time-domain approach towards general-purpose code development for sound propagation prediction with unstructured mesh, Proceedings of Inter-Noise 2008 (Shanghai), No. 287, 15 pages in CD-ROM, 2008.
The code is available at http://openfoamwiki.net/index.php/Contrib_potentialWaveFoam

A Full Finite-Volume Time-Domain Approach towards General-purpose Code Development for Sound Propagation Prediction with Unstructured Mesh

Takuya Oshima[1], Masashi Imano[2]
[1]Faculty of Engineering, Niigata University,
8050 Igarashi-Ninocho, Niigata City, 9502181, Japan
[2]School of Engineering, The University of Tokyo,
7-3-1 Hongo, Bunkyo-ku, Tokyo, 1138656, Japan

ABSTRACT

While finite-difference time-domain (FDTD) approach has widely been accepted as a simple, fast and proven measure for numerical sound propagation prediction, it has suffered enforcement of orthogonal mesh usage and lack of general-purpose solver code. Due to the weaknesses we even now have to write solvers and pre/postprocessing codes on case-by-case basis. This has made real industrial applications of the technique with complex geometries difficult. The issue was addressed here through introduction of a full finite-volume time-domain (FVTD) approach meant as a replacement for the FDTD technique. The main strength of the FVTD approach in principle is a great flexibility in mesh handlings which allows full unstructured meshes containing arbitrary shapes of polyhedra. Thus the strength opens possibility of using a vast variety of general-purpose pre/postprocessors designed for finite volume or finite element meshes. The proposed FVTD technique, along with an acoustic impedance boundary condition specifically developed for use with the technique, was formulated, implemented and tested using solutions obtained by the FDTD technique as benchmarks. Both techniques were confirmed to produce identical results under identical geometry, mesh and computational conditions. The demanded processor times and memory usages for FVTD calculations were more than ten times of FDTD calculations, which still was thought to be allowable up to medium-sized problems with recent advancements in processor performance taken into account. The results obtained under full unstructured tetrahedral meshes, however, showed numerical dispersions and diffusiveness, which indicated necessity of further works.

1 INTRODUCTION

While finite-difference time-domain (FDTD) approach has widely been accepted as a simple, fast and proven measure for numerical sound propagation prediction, it has suffered enforcement of orthogonal mesh usage and lack of general-purpose solver code.

[1]Email address: oshima@eng.niigata-u.ac.jp
[2]Email address: imano@arch.t.u-tokyo.ac.jp

Thus we even now often have to write solvers and pre- and postprocessing codes on case-by-case basis. The resultant negative effects arising from the shortcomings are mainly twofold:

1. With recent advancements in processor performance taken into account, the shortcomings has made relative cost of human powers with regard to pre- and postprocessings much higher than the cost devoted for numerical simulation itself, in particular for small- and medium-sized cases. The situation has made real industrial applications of the FDTD technique for complex geometries difficult.

2. Despite the wide use of the FDTD technique in many literatures, we still do not, and will not be able to, have a common case sharing framework for accumulating case examples which would stimulate communications between computational acousticians unless the circumstance changes.

On the other hand, if we were to propose a new approach as an alternative to the FDTD technique, we also have to keep in mind that the FDTD technique is so widely used since it does have its own strengths:

1. The FDTD technique is mathematically simple and thus easy to implement.

2. Thanks to the simplicity, its computational cost per cell is extremely low.

The possible new approach is expected to maintain these features at least to some extent.

All the issue was addressed here through introduction of a full finite-volume time-domain (FVTD) approach meant as a replacement for the FDTD technique, as opposed to a mixed finite-difference and finite-volume approach meant as a complement for handling body-fitted cells in FDTD computation [1]. The main strength of the full FVTD approach in principle is a great flexibility in mesh handlings which allows using unstructured meshes containing arbitrary shapes of polyhedra, while maintaining relative simplicity compared to other more advanced approaches such as BEM or FEM. Hence the strength opens possibility of using a vast variety of general-purpose pre- and postprocessors designed for finite volume or finite element meshes, keeping computational costs per cell relatively low at the same time.

To fully exploit the inherent feature of finite volume approach, the proposed technique has been implemented as a user application on top of an open-source finite volume based toolkit, OpenFOAM [2]. With this approach, not only the developers can make maximum use of its tried and proved finite volume operators and I/O libraries, but also a user can get full access to the included mesh format converters and postprocessing exporters.

The implementation was tested for contrasting its accuracy and computational costs against the FDTD approach. Furthermore, several formulations of the acoustic impedance boundary condition were carried out comparative tests under orthogonal and unstructured meshes to choose the accompanying implementation of the boundary condition with the main FVTD implementation.

2 FORMULATION AND IMPLEMENTATION

2.1 Finite-Volume Formulation

The wave propagation equation represented in velocity potential ϕ is written as the following equation.

$$\frac{\partial^2 \phi}{\partial t^2} = c_0^2 \nabla^2 \phi \tag{1}$$

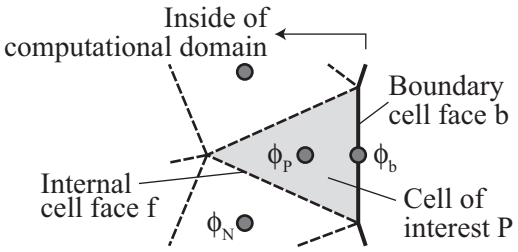

Figure 1: Unstructured mesh system.

where t, c_0, ∇^2 are time, propagation speed of the wave and Laplacian operator respectively. Using ϕ, pressure p and particle velocity $\boldsymbol{u}$ are written as follows.

$$p = \rho\frac{\partial\phi}{\partial t}, \tag{2}$$

$$\boldsymbol{u} = -\nabla\phi. \tag{3}$$

Eq. (1) is discretized under unstructured grid system as shown in Fig. 1 where the definition point of physical quantities are taken at the barycenter of each control volume (CV). For the left hand side of Eq. (1), by integrating over the CV with time-invariant volume V and applying central time-differential scheme, we get

$$\frac{\partial^2}{\partial t^2}\int_V \phi\, dV \approx \frac{\phi^{n+1} - 2\phi^n + \phi^{n-1}}{\Delta t^2}V$$

where ϕ^{n-1}, ϕ^n, ϕ^{n+1} denote the values of ϕ at the $(n-1)$-th, n-th, $(n+1)$-th steps of time step Δt. For the right hand side, by integrating Eq. (1) within a CV and applying divergence theorem, we get

$$\begin{aligned}\int_V c_0^2\,\nabla^2\phi dV &= c_0^2\int_S d\boldsymbol{S}\cdot\nabla\phi \\ &\approx c_0^2\sum_{\mathrm{f}}\boldsymbol{S}_{\mathrm{f}}\cdot(\nabla\phi)_{\mathrm{f}}\end{aligned} \tag{4}$$

where $\boldsymbol{S}_{\mathrm{f}}$ denotes the face area vector of the f-th face that constitutes polyhedral CV in question as follows.

$$\boldsymbol{S}_{\mathrm{f}} = S_{\mathrm{f}}\boldsymbol{n}_{\mathrm{f}} \tag{5}$$

where S_{f}, $\boldsymbol{n}_{\mathrm{f}}$ are the area and the unit outward normal vector of the face f respectively.

If a vector connecting the centers of the CV P and its adjacent CV N, $\boldsymbol{d}_{PN}$, is parallel to $\boldsymbol{S}_f$, $\boldsymbol{S}_{\mathrm{f}}\,(\nabla\phi)_{\mathrm{f}}$ is written in terms of $\partial\phi/\partial n_{\mathrm{f}}$, the surface-normal gradient of ϕ. Thus the term within the summation in the rightmost hand side of Eq. (4) is discretized as follows.

$$\begin{aligned}\boldsymbol{S}_{\mathrm{f}}\cdot(\nabla\phi)_{\mathrm{f}} &= S_{\mathrm{f}}\frac{\partial\phi}{\partial n_{\mathrm{f}}} \\ &\approx S_{\mathrm{f}}\frac{\phi_{\mathrm{N}} - \phi_{\mathrm{P}}}{|\boldsymbol{d}_{\mathrm{PN}}|}\end{aligned} \tag{6}$$

However, if $\boldsymbol{d}_{PN}$ is nonorthogonal to $\boldsymbol{S}_{\mathrm{f}}$, $\boldsymbol{S}_{\mathrm{f}}$ has to be decomposed into its orthogonal part $\boldsymbol{\Delta}_{\mathrm{f}}$ and nonorthogonal part $\boldsymbol{k}_{\mathrm{f}}$.

$$\boldsymbol{S}_{\mathrm{f}}\cdot(\nabla\phi)_{\mathrm{f}} = \boldsymbol{\Delta}_{\mathrm{f}}\cdot(\nabla\phi)_{\mathrm{f}} + \boldsymbol{k}_{\mathrm{f}}\cdot(\nabla\phi)_{\mathrm{f}}$$

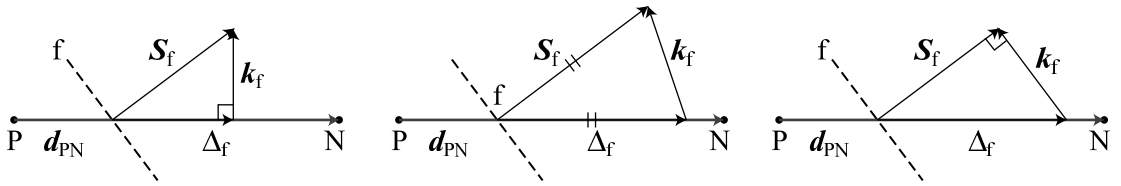

a) Underrelaxed correction b) Orthogonal correction c) Over-relaxed correction

Figure 2: Nonorthogonal mesh treatment vectors.

The first term of the right hand side of the equation above, the orthogonal part, is discretized similarly to Eq. (6) as follows.

$$\boldsymbol{\Delta}_{\mathrm{f}} \cdot (\nabla\phi)_{\mathrm{f}} \approx |\boldsymbol{\Delta}_{\mathrm{f}}| \, \frac{\phi_{\mathrm{N}} - \phi_{\mathrm{P}}}{|\boldsymbol{d}_{\mathrm{PN}}|}$$

The nonorthogonal part, $(\nabla\phi)_{\mathrm{f}}$ in the second term, is given by interpolating the gradient of ϕ at the centers of CVs P and N.

$$(\nabla\phi)_{\mathrm{f}} = f_x(\nabla\phi)_{\mathrm{P}} + (1 - f_x)(\nabla\phi)_{\mathrm{N}} \tag{7}$$

Here, the interpolation coefficient f_x and the gradient $(\nabla\phi)_{\mathrm{P}}$ are given as follows.

$$\begin{aligned} f_x &= \frac{\overline{\mathrm{fN}}}{|\boldsymbol{d}_{\mathrm{PN}}|}, \\ (\nabla\phi)_{\mathrm{P}} &= \frac{1}{V}\int_S d\boldsymbol{S}\,\phi \\ &\approx \frac{1}{V}\sum_{\mathrm{f}} \boldsymbol{S}\phi_{\mathrm{f}} \end{aligned}$$

where ϕ_{f} is a face-interpolated value of ϕ at the center of CVs.

2.2 Nonorthogonal Corrections for Laplacian Term

The orthogonal and nonorthogonal component vectors $\boldsymbol{\Delta}_{\mathrm{f}}$ and $\boldsymbol{k}_{\mathrm{f}}$ can be calculated arbitrarily. In the present paper we are comparing three techniques proposed by Jasak [3].

Underrelaxed correction:

$$\boldsymbol{\Delta}_{\mathrm{f}} = \frac{\boldsymbol{d}_{\mathrm{PN}} \cdot \boldsymbol{S}_{\mathrm{f}}}{|\boldsymbol{d}_{\mathrm{PN}}|^2}\boldsymbol{d}_{\mathrm{PN}} \tag{8}$$

Orthogonal correction:

$$\boldsymbol{\Delta}_{\mathrm{f}} = \frac{\boldsymbol{d}_{\mathrm{PN}}}{|\boldsymbol{d}_{\mathrm{PN}}|}S_{\mathrm{f}} \tag{9}$$

Overrelaxed correction:

$$\boldsymbol{\Delta}_{\mathrm{f}} = \frac{\boldsymbol{d}_{\mathrm{PN}}}{\boldsymbol{d}_{\mathrm{PN}} \cdot \boldsymbol{S}_{\mathrm{f}}}S_{\mathrm{f}}^2 \tag{10}$$

Jasak concludes overrelaxed correction to be the best correction technique as a result of testing the techniques with solutions of the Laplacian equation under 10°–60° skewed two

dimensional quadrilateral meshes. However, typical skewnesses for tetrahedral meshes, which most of meshing softwares support for three-dimensional geometries, typically fits in a relatively small range of under 20°. Furthermore, behaviors for the wave equation is not known. Hence the effectiveness of the techniques will be reinvestigated in the following section.

2.3 Rigid Boundary Conditions

On acoustically rigid boundaries b, normal component of particle velocity u_b is fixed to zero.

$$u_\mathrm{b} = \boldsymbol{n}_\mathrm{b} \cdot \boldsymbol{u}_\mathrm{b} = 0 \tag{11}$$

Substituting the relationship above to Eqs. (3) and (5) leads to the equation below which represents the surface normal gradient of ϕ being zero.

$$\boldsymbol{S}_\mathrm{b} \cdot (\nabla\phi)_\mathrm{b} = 0$$

2.4 Normal Incidence Acoustic Impedance Boundary Conditions

Acoustic impedance at boundaries under normal incidence condition z is given as

$$z = \frac{p}{u_\mathrm{b}},$$

where u_b is the normal component of particle velocity. Substituting Eqs. (2) and (3) to the equation above, we get an advection equation of velocity potential ϕ.

$$\frac{\partial\phi}{\partial n_\mathrm{b}} = -\frac{1}{c_\mathrm{b}}\frac{\partial\phi}{\partial t}, \tag{12}$$

where

$$c_\mathrm{b} = \frac{z}{\rho}.$$

The advection equation Eq. (12) has to be discretized to calculate the surface normal gradient of ϕ at the time step $n+1$ at the boundary face barycenter b shown in Fig. 1, namely $\partial\phi/\partial n_\mathrm{b}|^{n+1}$. In the deriving process of the discretized forms of Eq. (12), three discretization schemes are applied for each of time and spacial directions, which leads to nine combinations of schemes in total. The discretized equations are shown below, with ϕ subscripted by P and b being the values of ϕ at barycenters of boundary-internal CV and boundary face respectively and Δn being the distance between the barycenters. The abbreviated type name that appears in the subtitle of each formulation is referred to later in Section 4.

2.4.1 Upwind Types

Upwind types are derived regarding time derivatives at P as approximations of those at b.

Central differencing formulation (Type U-C) The formulation is obtained by applying a second order central differencing scheme to the time derivative of Eq. (12).

$$\left.\frac{\partial\phi}{\partial n_\mathrm{b}}\right|^{n+1} = -\frac{1}{c_\mathrm{b}}\frac{\phi_\mathrm{P}^{n+1} - \phi_\mathrm{P}^{n}}{\Delta t} \tag{13}$$

Second-order backward formulation (Type U-B) The formulation is obtained by applying second order backward differencing scheme [4] to the time derivative.

$$\left.\frac{\partial\phi}{\partial n_\mathrm{b}}\right|^{n+1} = -\frac{1}{c_\mathrm{b}}\frac{3\phi_\mathrm{P}^{n+1}-4\phi_\mathrm{P}^{n}+\phi_\mathrm{P}^{n-1}}{2\Delta t} \tag{14}$$

Crank-Nicholson type formulation (Type U-CN) Crank-Nicholson interpolation scheme is applied to obtain the spatial derivative of Eq. (12) at time step $n+1/2$, while the time derivative is discretized with a second order differencing scheme.

$$\frac{1}{2}\left(\left.\frac{\partial\phi}{\partial n_\mathrm{b}}\right|^{n+1} + \left.\frac{\partial\phi}{\partial n_\mathrm{b}}\right|^{n}\right) = -\frac{1}{c_\mathrm{b}}\frac{\phi_\mathrm{P}^{n+1}-\phi_\mathrm{P}^{n}}{\Delta t} \tag{15}$$

By reducing the equation above, we have a recurring formula with regard to the spatial derivative.

$$\left.\frac{\partial\phi}{\partial n_\mathrm{b}}\right|^{n+1} = -\frac{2}{c_\mathrm{b}}\frac{\phi_\mathrm{P}^{n+1}-\phi_\mathrm{P}^{n}}{\Delta t} - \left.\frac{\partial\phi}{\partial n_\mathrm{b}}\right|^{n} \tag{16}$$

2.4.2 Predictor-Corrector Types

As noted above, the spatial derivative values $\partial\phi/\partial n_\mathrm{b}|^{n+1}$ obtained by Eqs. (13), (14) and (16) are in fact those at the CV barycenter P, $\partial\phi/\partial n_\mathrm{b}|_\mathrm{P}^{n+1}$. To extrapolate the value to the boundary b, we first calculate a predictor with

$$\phi_*^{n+1} = \phi_\mathrm{P}^{n+1} + \left.\frac{\partial\phi}{\partial n_\mathrm{b}}\right|_\mathrm{P}^{n+1}\Delta n, \tag{17}$$

and then apply a predictor-corrector scheme [4] to the surface-normal direction to obtain the surface gradient $\partial\phi/\partial n_\mathrm{b}|^{n+1}$.

Central differencing formulation (Type PC-C) First we calculate the predictor similarly to the upwind formulation, Eq. (13),

$$\left.\frac{\partial\phi}{\partial n_\mathrm{b}}\right|_\mathrm{P}^{n+1} = -\frac{1}{c_\mathrm{b}}\frac{\phi_\mathrm{P}^{n+1}-\phi_\mathrm{P}^{n}}{\Delta t}$$

and then we obtain a corrected value, by way of Eq. (17), as follows.

$$\left.\frac{\partial\phi}{\partial n_\mathrm{b}}\right|^{n+1} = \frac{1}{2}\left(\left.\frac{\partial\phi}{\partial n_\mathrm{b}}\right|_\mathrm{P}^{n+1} - \frac{\phi_*^{n+1}-\phi_\mathrm{b}^{n}}{c_\mathrm{b}\Delta t}\right)$$

ϕ_b^n in the equation above is calculated by the following equation (the same applies hereafter).

$$\phi_\mathrm{b}^n = \phi_\mathrm{P}^n + \left.\frac{\partial\phi}{\partial n_\mathrm{b}}\right|^{n}\Delta n \tag{18}$$

Second-order backward formulation (Type PC-B) Similarly to Eq. (14), we obtain a predictor

$$\left.\frac{\partial\phi}{\partial n_\mathrm{b}}\right|_\mathrm{P}^{n+1} = -\frac{3\phi_\mathrm{P}^{n+1}-4\phi_\mathrm{P}^{n}+\phi_\mathrm{P}^{n-1}}{2c_\mathrm{b}\Delta t},$$

followed by a corrected value by way of Eq. (17),

$$\left.\frac{\partial\phi}{\partial n_\mathrm{b}}\right|^{n+1} = \frac{1}{2}\left(\left.\frac{\partial\phi}{\partial n_\mathrm{b}}\right|_\mathrm{P}^{n+1} - \frac{3\phi_*^{n+1}-4\phi_\mathrm{b}^{n}+\phi_\mathrm{b}^{n-1}}{2c_\mathrm{b}\Delta t}\right).$$

Crank-Nicholson type formulation (Type PC-CN) By replacing $\partial\phi/\partial n_\mathrm{b}|^n$ in the corresponding upwind formulation to $\partial\phi/\partial n_\mathrm{b}|_\mathrm{P}^n$, we obtain

$$\left.\frac{\partial\phi}{\partial n_\mathrm{b}}\right|_\mathrm{P}^{n+1} = -\frac{2}{c_\mathrm{b}}\frac{\phi_\mathrm{P}^{n+1}-\phi_\mathrm{P}^{n}}{\Delta t} - \left.\frac{\partial\phi}{\partial n_\mathrm{b}}\right|_\mathrm{P}^{n}$$

followed by a corrected value by way of Eq. (17),

$$\left.\frac{\partial\phi}{\partial n_\mathrm{b}}\right|^{n+1} = \frac{1}{2}\left(\left.\frac{\partial\phi}{\partial n_\mathrm{b}}\right|_\mathrm{P}^{n+1} - \frac{2}{c_\mathrm{b}}\frac{\phi_*^{n+1}-\phi_\mathrm{b}^{n}}{\Delta t} - \left.\frac{\partial\phi}{\partial n_\mathrm{b}}\right|^{n}\right).$$

2.4.3 Algebraic Types

The left hand side in Eq. (12) is discretized as

$$\left.\frac{\partial\phi}{\partial n_\mathrm{b}}\right|^{n+1} = \frac{\phi_\mathrm{b}^{n+1}-\phi_\mathrm{P}^{n+1}}{\Delta n}$$

while the right hand side is discretized at the boundary surface b. Then we can obtain $\left(\phi_\mathrm{b}^{n+1}-\phi_\mathrm{P}^{n+1}\right)/\Delta n$, namely the second order differentiated form of $\partial\phi/\partial n_\mathrm{b}|^{n+1}$, by algebraic reduction.

Central differencing formulation (Type A-C) By discretizing both sides of Eq. (12), we obtain

$$\frac{\phi_\mathrm{b}^{n+1}-\phi_\mathrm{P}^{n+1}}{\Delta n} = -\frac{1}{c_\mathrm{b}}\frac{\phi_\mathrm{b}^{n+1}-\phi_\mathrm{b}^{n}}{\Delta t}.$$

After approximating $\left(\phi_\mathrm{b}^{n+1}-\phi_\mathrm{P}^{n+1}\right)/\Delta n$ to $\partial\phi/\partial n_\mathrm{b}|^{n+1}$, the equation above is reduced to

$$\left.\frac{\partial\phi}{\partial n_\mathrm{b}}\right|^{n+1} = \frac{\phi_\mathrm{b}^{n}+\phi_\mathrm{P}^{n+1}}{c_\mathrm{b}\Delta t+\Delta n}$$

Second-order backward formulation (Type A-B) Similarly to Type A-C, we obtain

$$\left.\frac{\partial\phi}{\partial n_\mathrm{b}}\right|^{n+1} = \frac{4\phi_\mathrm{b}^{n}-\phi_\mathrm{b}^{n-1}-3\phi_\mathrm{P}^{n}}{2c_\mathrm{b}\Delta t+3\Delta n}.$$

Crank-Nicholson type formulation (Type A-CN) Similarly to Type A-C, we obtain

$$\frac{1}{2}\left(\frac{\phi_{\mathrm{b}}^{n+1}-\phi_{\mathrm{P}}^{n+1}}{\Delta n}+\left.\frac{\partial\phi}{\partial n_{\mathrm{b}}}\right|^{n}\right)=-\frac{1}{c_{\mathrm{b}}}\frac{\phi_{\mathrm{b}}^{n+1}-\phi_{\mathrm{b}}^{n}}{\Delta t}$$

and its final reduced form

$$\left.\frac{\partial\phi}{\partial n_{\mathrm{b}}}\right|^{n+1} = \frac{2}{c_{\mathrm{b}}\Delta t+2\Delta n}\left(\phi_{\mathrm{b}}^{n}-\phi_{\mathrm{P}}^{n+1}\right)-\frac{c_{\mathrm{b}}\Delta t}{c_{\mathrm{b}}\Delta t+2\Delta n}\left.\frac{\partial\phi}{\partial n_{\mathrm{b}}}\right|^{n}. \tag{19}$$

3 TESTS FOR VALIDATION AND NONORTHOGONAL CORRECTION TECHNIQUES

3.1 Computational Setups

To validate the proposed FVTD technique and to test the correction techniques under unstructured meshes, a comparative test using a sound propagation problem in a closed cube of 1 m × 1 m × 1 m, one of the AIJ-BPCA (Benchmark Platform on Computational Methods for Architectural and Environmental Acoustics) [5] problems, was carried out. The detail of the tested cases are shown in Tab. 1.

Case 1 The problem was solved using a conventional FDTD code written in Fortran 77 employing a pressure-particle velocity leapfrog scheme. The case is meant to be the benchmark case to which the results obtained by the proposed technique is compared for validation. Each edge of the cube was divided to 81 subedges to create a mesh of cell width $\Delta x = 0.0123$ m and the number of cells 531 441 (Fig. 3(b)). The time step Δt and the Courant number C_o were set to 0.02 ms and 0.96 respectively.

Case 2 The problem was solved with the proposed technique under a hexahedral orthogonal mesh and setup both identical to the ones for Case 1.

Case 3 The problem was solved with the proposed technique under a nonuniform tetrahedral unstructured mesh automatically generated by an open-source mesher, Gmsh [6]. The characteristic length l_c (the length with which each edge of the cube is divided) is set to 0.025 m, to make a mesh with the number of CVs 531 333 (roughly the same as Cases 1 and 2). The ratio of maximum and minimum CV edge lengths of the generated mesh was 6.32. The time step Δt was set to 0.0049 ms to keep the maximum Courant number to 0.99. In this case no nonorthogonal techniques were applied.

Cases 4, 5 and 6 The setups are same as Case 3, except that the underrelaxed, orthogonal and overrelaxed nonorthogonal correction techniques were applied to Cases 4, 5 and 6 respectively.

Common Conditions For all cases the initial values of ϕ were set to represent the pressure and particle velocity conditions of

$$p^{-1/2}(r) = \begin{cases}\dfrac{\cos 8\pi r+1}{2} & (r<0.125)\\ 0 & (\text{otherwise})\end{cases}\ [\mathrm{Pa}] \tag{20}$$

$$\boldsymbol{u}^{0}(r) = \mathbf{0} \tag{21}$$

where r [m] is the distance from the center of the cube. All cases were run up to $t = 0.04$s.

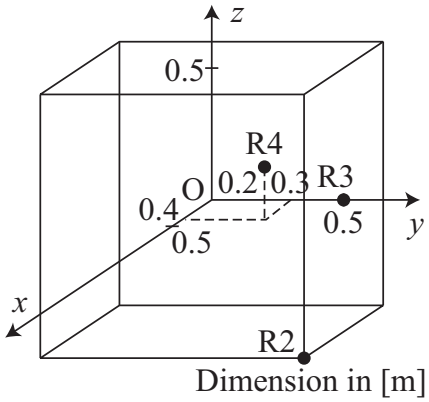

(a) Problem geometry

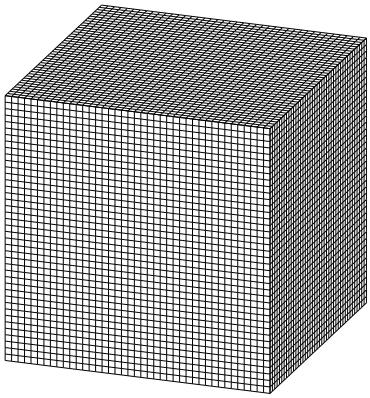

(b) Surface (Hexahedral)

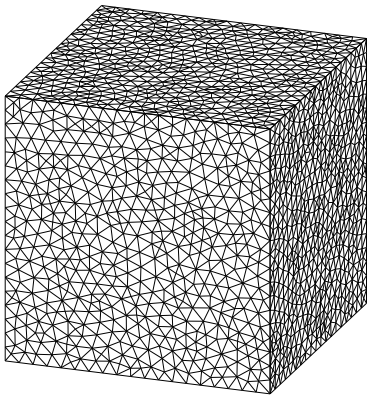

(c) Surface (Tetrahedral)

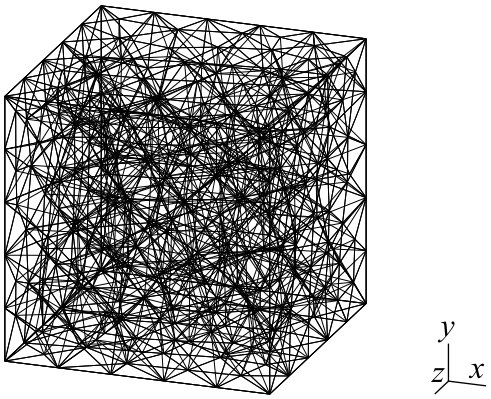

(d) Internal (Tetrahedral)

Figure 3: (a) Problem geometry of the benchmark problem AIJ-BPCA B0-1T, (b) Surface mesh for Cases 1 and 2 (coarsened by factor of 2 for visibility), (c) Surface mesh for Cases 3–6 (coarsened by factor of 2) and (d) Surface and internal mesh (coarsened by factor of 8) for Cases 3–6.

Table 1: Computational setups.

Case	1	2	3	4	5	6
Approach	FDTD	FVTD				
Type of mesh	—	Hexahedral	Unstructured tetrahedral			
Number of cells/CVs	$81^3 = 531\,441$		531 333			
Δx [m]	0.0123		—			
l_c [m]	—		0.025 (40 elements per edge)			
Δt [ms]	0.02		0.0049			
c_0 [m/s]	343.7					
Courant number	0.96		0.99 (max)			
Nonorth. correction	—	Uncorrected	Underrelaxed	Orthogonal	Overrelaxed	
Initial condition	A single wave of offset cosine (Eqs. (20), (21))					

3.2 Results and Discussions

The transient sound pressure waveforms at the receiving point R2 shown in Fig. 3(a) are plotted in Fig. 4, using the result of Case 1 as the benchmark case for comparison with other cases. From Fig. 4(a), one can see that the results of FDTD and FVTD

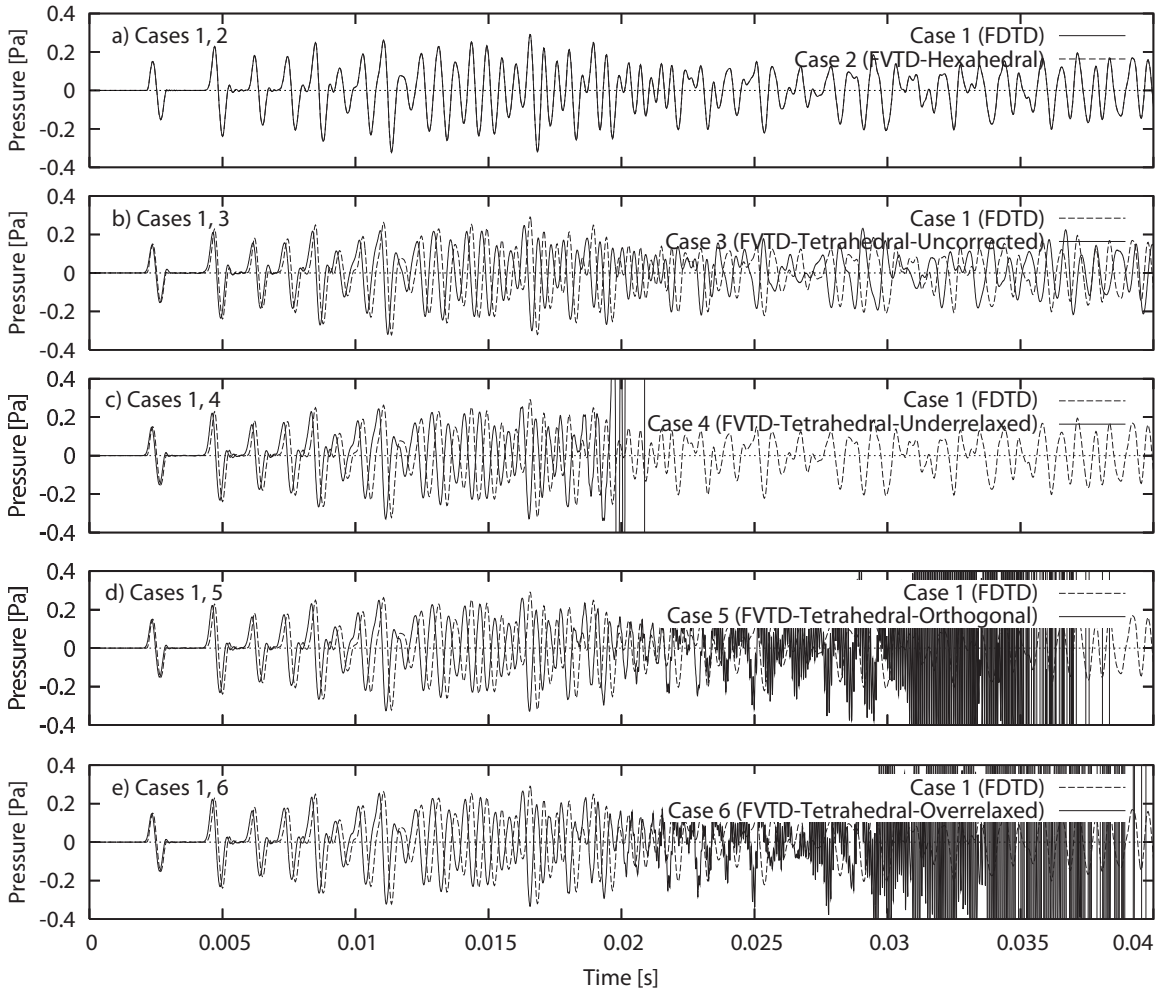

Figure 4: Transient sound pressure waveforms at the receiving point R2.

techniques agrees so precisely that they can be regarded as virtually identical results. From the results one can verify the proposed FVTD technique has the same accuracy as a conventional FDTD under identical geometry, mesh and computational setups.

On the other hand, from the comparison of Cases 1 and 3 in Fig. 4(b), the waveform obtained by the FVTD technique under the tetrahedral mesh is phasing forward in about 1.5 % and the overall waveform is gradually dispersing over time. In addition, the results of Cases 4–6, which were meant to confirm the effects of the correction techniques to correct the unwanted behavior observed in Case 3, are shown in Fig. 4(c)–(e) respectively. Despite the employment of the correction techniques, the drifts of the phase did not improve, or even worse, waveforms started to oscillate and diverge eventually. Although the starting times of the oscillations become slightly later for relaxed cases, the overall characteristics do not differ much.

From the results one can conclude that while one can expect identical results between FDTD and FVTD techniques under identical setups, there remains works for the FVTD technique in reducing the phase error coming from nonorthogonalities of unstructured grids.

Table 2: Processor and memory usages.

Case	1	2	3	4
Processor [s]	28.0	343	865	2 013
Per time step [s]	0.0140	0.172	0.106	0.247
Memory [MB]	18	301	260	260

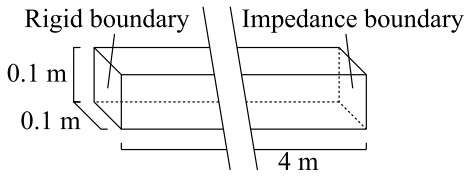

Figure 5: Geometry of one-dimensional tube.

3.3 Computational Loads

To compare the proposed technique with the conventional FDTD from the standpoint of computational loads, processor times and memory usages were instrumented for Cases 1–4, as shown in Tab. 2. The instrumentations were carried out on an Opteron 2.4 GHz 64-bit Linux platform. The FVTD computations turned out to require more than ten times for processor and memory usages. Hence it should be noted that, from the computational load of view, the proposed FVTD technique is not meant to completely replace FDTD especially in large cases, but should rather be used for small to medium cases where rapid preprocessing (case setup) and postprocessing have of particular importance.

Although Cases 2 and 3 have roughly the same number of cells, one may notice that Case 3 requires smaller amount of computational time per time step. This is because the computational load required in calculating Laplacian is determined mostly by the number of faces per CV, as shown in Eq. (4). It is also shown that, from Cases 3 and 4, applying nonorthogonal correction technique more than doubles the processor usage.

4 COMPARATIVE TESTS FOR THE ACOUSTIC IMPEDANCE BOUNDARY CONDITION

The nine different formulations of the normal acoustic impedance boundary condition proposed in Section 2.4 were tested under an acoustic tube as a one dimensional problem, square-shaped domain as a two-dimensional problem, and an eighth of a sphere as a three-dimensional problem.

4.1 One-dimensional Tests

4.1.1 Computational Setups

To test the formulations under normal incidence conditions, an acoustic tube shown in Fig. 5 was uniformly meshed with Δx being 0.1 m. The right end of the tube was employed an impedance boundary condition with the characteristic impedance of the air, ρc_0. All other boundaries were set to have been rigid. The time step Δt was set to 0.291 ms which corresponds to the Courant number of 1.0. The half wave of a cosine pulse with the wavelength $5\Delta x$ was given at the left end of the tube as an initial condition.

4.1.2 Results

Total acoustic energy levels in the tube over time were shown in Fig. 6. The formulation that corresponds to each Type is defined in Section 2.4. Types U-C, PC-CN and A-CN similarly show good attenuations after $t = 0.01$ s, when the absorption of the wavefronts that reached the right end of the tube starts. On the other hand, Types

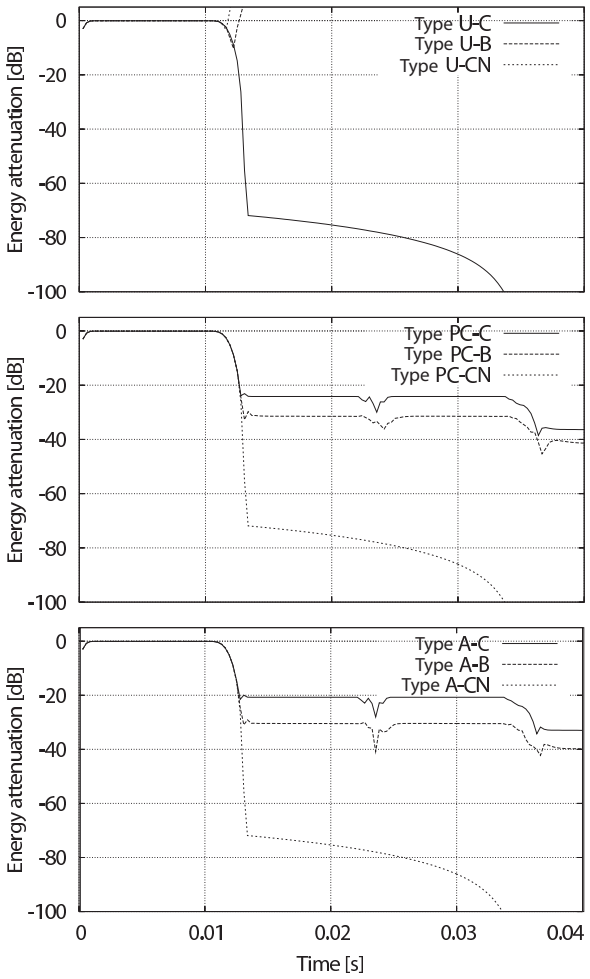

Figure 6: Attenuation of total acoustic energy in the tube over time.

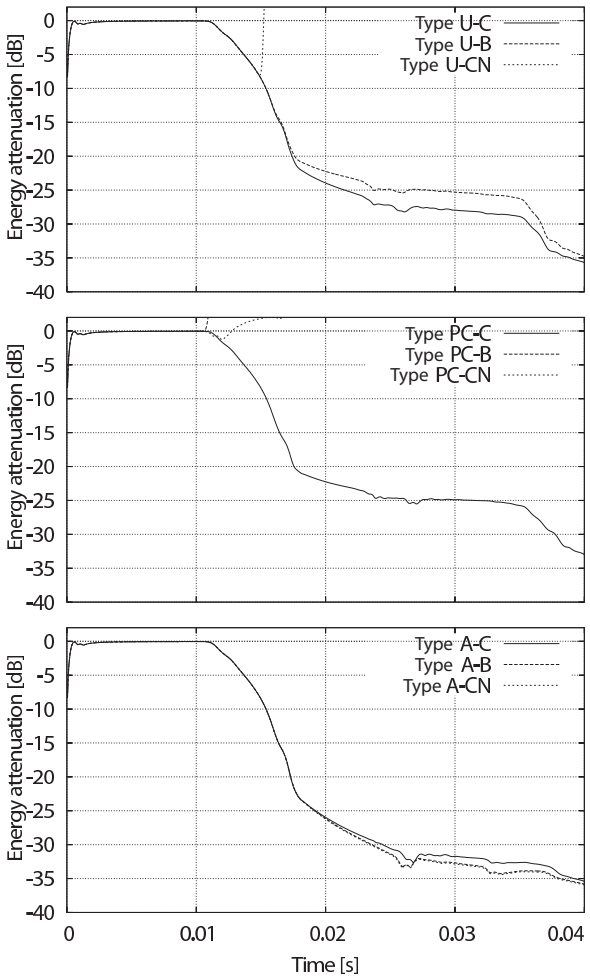

Figure 7: Attenuation of total acoustic energy in the square domain over time (Δt = 0.05 ms).

PC-C, PC-B, A-C and A-B only show smaller attenuation than the former three types. Furthermore Types U-B and U-CN quickly diverged as soon as the wavefronts reached the right end.

4.2 Two-dimensional Tests

4.2.1 Setup

Following the reference [7], an acoustic wave propagation problem in a flat square domain was solved. The geometry shown in Fig. 10 was orthogonally meshed with the cell width 0.05 m. Acoustic impedance boundary condition with the characteristic impedance of the air, ρc_0, was given for all edges. The time step Δt was set to two values of 0.05 ms and 0.1 ms, which correspond to the Courant numbers of 0.486 and 0.972. A cosine pulse with its radius being 10 times the cell width was given at the center of the square.

4.2.2 Results

Total acoustic energy in the field over time are plotted in Figs. 7 and 8 for $\Delta t = 0.05$ ms and 0.1 ms respectively. When $\Delta t = 0.05$ ms, the energies diverged for Types U-CN, PC-B and PC-CN. It can be seen that types that employed higher order schemes in

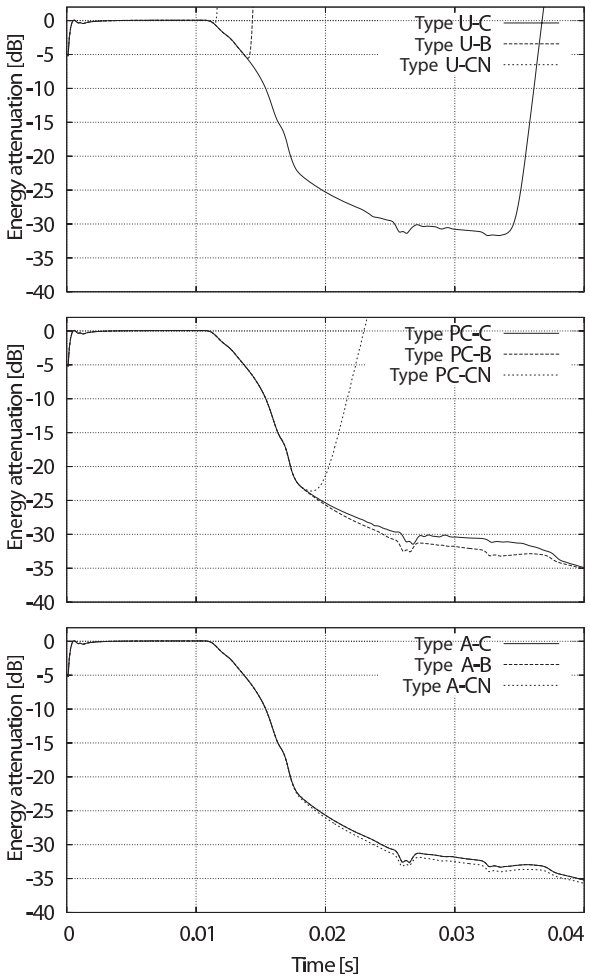

Figure 8: Attenuation of total acoustic energy in the square domain over time ($\Delta t = 0.1$ ms).

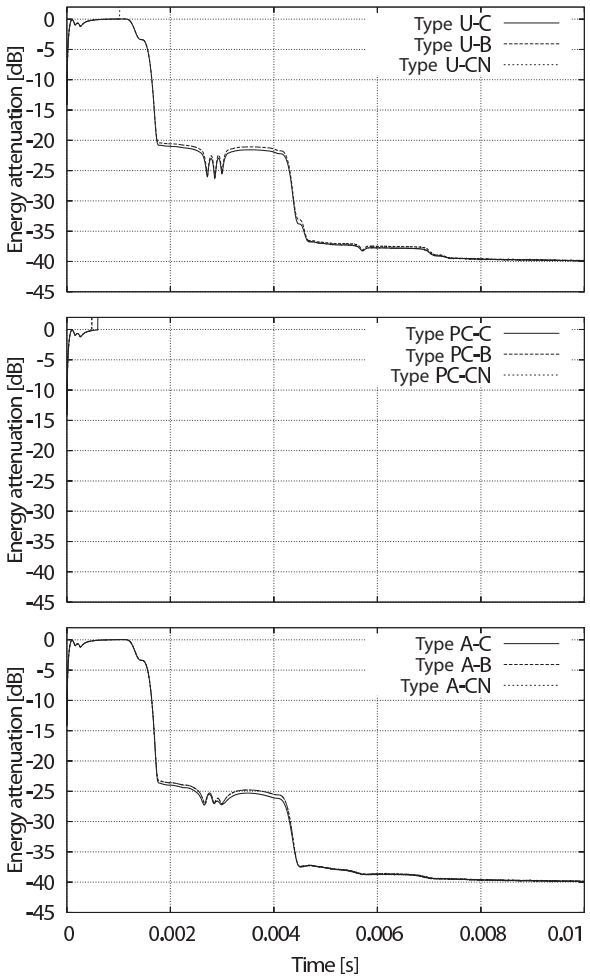

Figure 9: Attenuation of total acoustic energy in the eighth of a sphere over time.

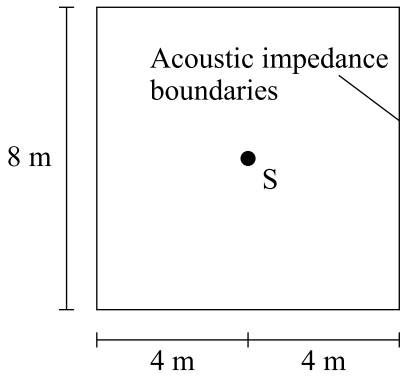

Figure 10: Geometry of computational domain.

a given formulation type have a tendency of divergence, except for the algebraic types which did not diverge (Types A-C, A-B, A-CN). On the contrary, when $\Delta t = 0.1$ ms, all types of the upwind type (Types U-C, U-B, U-CN) and Type PC-CN diverged. Again, no divergence was observed for the algebraic type. Especially Type A-CN showed the best attenuation of -35 dB at $t = 0.04$ s, and the variation between the results of $\Delta t = 0.05$ ms and 0.1 ms was smallest among the all types.

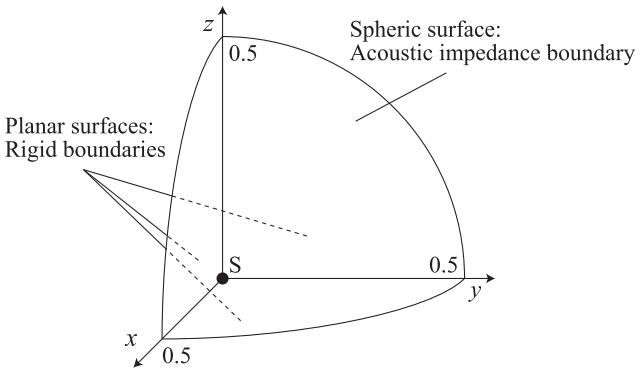

Figure 11: Geometry of eighth-spherical computational domain.

4.3 Three-dimensional Tests

4.3.1 Setup

To test the boundary conditions under a three-dimensional problem, an eighth of a sphere shown in Fig. 11 was meshed with tetrahedral cells of characteristic length $l_c = 0.0125$ m. The spherical surface was given an acoustic impedance boundary condition with characteristic impedance of the air, ρc_0. Rigid boundary conditions was imposed for other boundary surfaces. Time step Δt was set to 2.36×10^{-5} s which corresponds to the maximum Courant number of 0.99. The calculations were run up to 0.01 s. A cosine pulse of radius 0.125 m was given at the center of the sphere (point S shown in Fig. 11) as the initial condition.

4.3.2 Results

The results are shown in Fig. 9 as total energy attenuations in the sound fields over time. All of the predictor-corrector types (Types PC-C, PC-B, PC-CN) and Type U-CN resulted in divergence. In the remaining converged types, the algebraic types showed better attenuations in 2–3 dB than the upwind types at $t = 0.002$ s where the spherical wave reaches the spherical boundary surface. Within the algebraic types Type A-C indicates slightly better attenuation in about 0.5 dB.

4.4 Discussion

Looking through all the tests under one-, two- and three- dimensional geometries, in overall the algebraic types have good characteristics in that in most tests they show good attenuation characteristics, and in that even in worst tests they do not diverge. Further, of the three algebraic types, Type A-CN was among the best types in one- and three-dimensional tests, and the unarguable best under two dimensional tests. Thus one can conclude Type A-CN as the best performing formulation for the normal acoustic impedance boundary condition.

5 CONCLUSIONS

To overcome several inherent shortcomings in the currently widely used FDTD-based sound propagation technique, such as enforced usage of orthogonal meshes and lack of general-purpose solver code, the authors presented a fully finite-volume time-domain (FVTD) approach. The proposed FVTD technique, along with an acoustic impedance boundary condition specifically developed for use with the technique, was formulated and implemented on top of an open-source finite volume based toolkit, OpenFOAM. The implementation was tested using solutions obtained by the FDTD technique as benchmarks.

Both techniques were confirmed to produce identical results under identical geometry, mesh and computational conditions. The demanded processor times and memory usages for FVTD calculations were more than ten times of FDTD calculations, which still was thought to be allowable up to medium-sized problems with recent advancements in processor performance taken into account. The boundary condition proved to show good attenuations on one-, two- and three-dimensional meshes including an unstructured mesh. The overall results obtained under full unstructured tetrahedral meshes, however, showed numerical dispersions and diffusiveness, despite of nonorthogoanl corrections. The nonorthogoanl correction problems indicated necessity of further works.

ACKNOWLEDGEMENTS

Parts of the work were supported by JSPS Grant-in-Aid for Scientific Research (A) 19206062, (B) 19360264 and by MEXT Grant-in-Aid for Young Scientists (B) 19760402.

REFERENCES

[1] Botteldooren, D. Acoustical finite-difference time-domain simulation in a quasi-cartesian grid. *J. Acoust. Soc. Am.*, Vol. 95, No. 5, pp. 2313–2319, 1994.5.

[2] Weller, H. G., Tabor, G., Jasak, H., and Fureby, C. A tensorial approach to computational continuum mechanics using object-oriented techniques. *Computers in Physics*, Vol. 12, No. 6, pp. 620–631, December 1998.

[3] Jasak, H. *Error analysis and estimation for the finite volume method with applications to fluid flows*. PhD thesis, Imperial College, June 1996.

[4] Ferziger, J. H. and Perić, M. *Computational Methods for Fluid Dynamics*. Springer-Verlag (Berlin), 1996. (Japanese version).

[5] Architectural Institute of Japan. Benchmark platform on computational methods for architectural / environmental acoustics. http://gacoust.hwe.oita-u.ac.jp/AIJ-BPCA/.

[6] Geuzaine, C. and Remacle, J.-F. Gmsh: a three-dimensional finite element mesh generator with built-in pre- and post-processing facilities. http://www.geuz.org/gmsh/.

[7] Naito, Y., Yokota, T., Sakamoto, S., and Tachibana, H. The study of complete absorption boundary for open region calculation by FDM. *Proc. The 2000 autumn meeting of the Acoustical Society of Japan*, Vol. II, pp. 751–752, September 2000.